Polarization-Related Optical Multistability and Chaos

京大超高層電波研究センター

北野正雄 （Masao KITANO）
藪崎 努 （Tsutomu YABUZAKI）
小川 徹 （Toru OGAWA）

I. INTRODUCTION

The phenomenon of chaos has been the subject of intense interest in the last few years. It is now recognized as a common phase of nonlinear dynamical system in addition to the conventional phases of stationary equilibrium and periodic (or quasi-periodic) oscillation. Since Ikeda et al.[1] have predicted chaotic behaviors in an optically bistable system, many theoretical and experimental studies have been made.[2-5] Optical system is a suitable material to study nonlinear phenomena including chaos because it has tractable theoretical models and precise experiments are possible. If neccessary, we can provide moderate complexities to it.[6,7] Along this line, we have proposed an optical system which utilizes interactions between right- and left-circularly polarized light beams through J = 1/2 to J = 1/2 transition.[8] We have shown that symmetry breaking and optical tristability are possible for this system. Since then, various kind of phenomena have been predicted[4,9] and some of them have been demonstrated experimentally.[10]

Recently we proposed a new version of such polarization-related bistable system that utilizes the optically-induced Faraday effect and needs no optical cavity.[11] We also performed the experiment by using a sodium cell and a multi-mode dye laser tuned

to a wing of the D_1 line.[12] An interesting feature of the system
is that it exhibits the most typical pitchfork bifurcation which
breaks the polarization symmetry. Namely the symmetry breaking
bifurcation is of a supercritical type, while in the tristable
system[8] it is of a subcritical type. In this paper we investigate
on the delay induced chaos in this optical system. When we
increase the input light intensity passing over the first
bifurcation, chaoic state having polarization asymmetry appears.
If we increase the intensity still more, fully-developed symmetric
chaos is reached. Thus we are interested in the bifurcation which
lies between those two states. As we will see later, the symmetry
recovering occurs through a sudden change of the chaotic
attractors. Recently Grebogi et al.[13] have introduced a new class
of bifurcation named 'crises of chaos', where the size of chaotic
attractor suddenly changes. We'll show that in our case the
symmetry is recovered through the crisis.

In Sec. II, we show the setup of the system and derive the
system equation which is a one dimensional difference-differential
equation having symmetry with respect to the exchange of two
circular polarizations. In Sec. III, we discuss on a one
dimensional map model and show a simple example of symmetry
recovering crisis. In Sec. IV, we describe the experimental setup
of electronic circuit to simulate the optical system. In the
experiment we observe three distinct types of symmetry recovering
crises. In Sec. V, we introduce a two dimensional map model to
explain the experimental results. Although the model seems to be
oversimplified to approximate our system in infinite dimensional
space, it can reproduce all of the three types of crises. We
present the strange attractors near crises for each type, and

discuss how they recover the symmetry. As we will see, unstable fixed points play important roles in crises. Finally, we summarize our results and discuss the remaining questions.

II. THE SYSTEM EQUATION

We consider an optically bistable system shown in Fig. 1. It is largely the same as the one in Refs. 11 and 12 except that a delay in the feedback is introduced by taking a large distance L
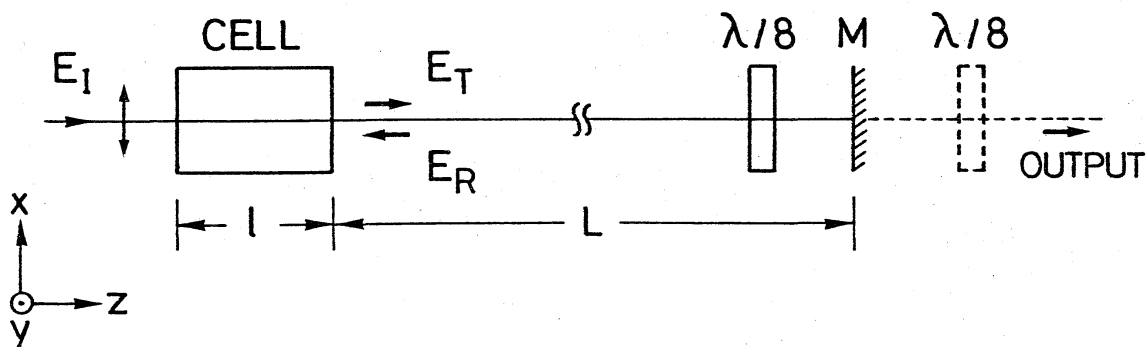

Fig. 1. Schematic illustration of the optically bistable system without an optical cavity.

between the cell and the mirror (M). Following the model adopted for the previous studies,[8,11,12] we consider spin-1/2 atoms which are optically pumped by the incident and the reflected light beams which are tuned to the wing of the resonance line. The state of the ensemble of atoms can be characterized by the magnetization component M_z along the optical axis, which is proportional to the population difference between $m_J = 1/2$ and $m_J = -1/2$ sublevels in the ground state. The time evolution of M_z is described by the Bloch equation:

$$\frac{dM_z}{dt} = - (\Gamma + I_+ + I_-)M_z + (I_+ - I_-)M_0, \tag{1}$$

where Γ is the relaxation rate of the magnetization and $I_{\pm}$ are the $\sigma_{\pm}$ light intensities which are normalized as to give pumping rates. If I_+ (I_-) is large enough compared to I_- (I_+) and Γ, all atoms are oriented along $+z$ $(-z)$ direction and the maximum polarization $M_z = M_0$ $(-M_0)$ is attained.

The absorption coefficients $\alpha_{\pm}$ and the wavenumber $k_{\pm}$ for $\sigma_{\pm}$ light are determined by the normalized magnetization component $m_z = M_z/M_0$ as

$$\alpha_{\pm} = \alpha(1 \mp m_z), \tag{2}$$

$$k_{\pm} = k_0 + \kappa(1 \mp m_z), \tag{3}$$

where α and κ are the absorption coefficeint and the incremental wavenumber for the unpolarized $(m_z = 0)$ medium respectively, and k_0 is the wavenumber in vacuum. In the dispersion regime we can neglect the absorption losses.

The polarization plane of the linearly-polarized incident light is rotated by an angle θ when the difference between k_+ and k_- exists (Faraday rotation). If we represent the incident light field as $\vec{E}_I = \sqrt{I_0}\hat{x}$, the transmitted field $\vec{E}_T$ is given by

$$E_T = \sqrt{I_0}(\hat{x} \cos \theta + \hat{y} \sin \theta), \tag{4}$$

$$\theta(t) = (k_- - k_+)l/2 = m_z(t)\kappa l, \tag{5}$$

where l is the length of the cell, and $\hat{x}$ and $\hat{y}$ are the unit

vectors.

The transmitted light is reflected by the mirror M set at a distance L and is fed back to the cell. Thus the feedback is delayed by the amount $t_R = 2L/c$. In the feedback path, a $\lambda/8$-plate is inserted whose optic axis is oriented to the x axis. By its action, the polarization state of the light fed back to the cell becomes

$$\vec{E}_R = \sqrt{I_{R+}}\,\hat{e}_- - \sqrt{I_{R-}}\,\hat{e}_+ , \tag{6}$$

$$I_{R\pm} = RI_0[1 \pm \sin 2\theta(t - t_R)]/2 , \tag{7}$$

where $\hat{e}_\pm = (-\hat{x} \pm i\hat{y})/\sqrt{2}$ and R is the reflectivity of the mirror. The $\sigma_\pm$ components of the reflected light suffer complementary modulations according to $\sin 2\theta(t - t_R)$. Experimentally the polarization state of $\vec{E}_R$ can be observed by monitoring the output light transmitting through the mirror M and an auxiliary $\lambda/8$-plate. We can also monitor the polarization state $\vec{E}_T$ by setting the fast axes of two $\lambda/8$-plates to form right angles. From Eqs. (7) and (5) we have the light intensities in the cell

$$I_\pm = I_0 [1 \pm R \sin 2\kappa l m_z(t - t_R)] . \tag{8}$$

Substitution Eq. (8) into Eq. (1) gives the system equation:

$$\frac{dm_z}{dt} = - (\Gamma + 2I_0)m_z(t) + RI_0\sin 2\kappa l m_z(t - t_R) . \tag{9}$$

Changing the time scale by $t' = \gamma^{-1}(\Gamma + 2I_0)t$ and introducing a new variable $X(t') = 2\kappa l m_z(t)$, we have a normalized form:

$$\gamma^{-1} \frac{dX}{dt'} = -X(t') + \mu \sin X(t' - t_R'), \qquad (10)$$

where $\mu = 2\kappa l R I_0 / (\Gamma + 2I_0)$ and $t_R' = \gamma^{-1}(\Gamma + 2I_0)t_R$. In the case $\Gamma \gg I_0$, μ is proportional to I_0 and t_R' is independent of I_0. In the experiment we can vary $t_R'\gamma$ by changing the length L or the relaxation rate Γ. Hereafter we drop the primes in t' and t_R'. When $t_R\gamma = 0$, Eq. (10) is an ordinary differential equation in one dimension, while in the limit $t_R\gamma \gg 1$, the system can be described by a difference equation as described in the next section. Therefore the parameter $t_R\gamma$ represents whether Eq. (10) is close to a difference equation or to a differential equation.

Note that Eq. (10) is invariant under the transformation $X \to -X$, which corresponds to the exchange of the roles of the spin-up and -down atoms, and the right- and left-circular polarized light.

III. THE ONE DIMENSIONAL MAP MODEL

In the limiting case $t_R\gamma \gg 1$, we can formally reduce Eq. (10) to the difference equation:

$$X_{n+1} = \mu \sin X_n, \qquad (11)$$

which defines a iteration of one dimensional map. As is well known,[2,3,14] this equation give an adequate qualitative prediction for the bifurcation structure for Eq. (10) with $t_R\gamma \gg 1$.

Figure 2 shows the bifurcation diagram for Eq. (11). For $\mu < \mu_0 = 1$, there exists only one stable fixed point $X = 0$. At $\mu = \mu_0$ a pitchfork bifurcation occurs at which the solution $X = 0$ becomes unstable and symmety breaking transition takes place. This
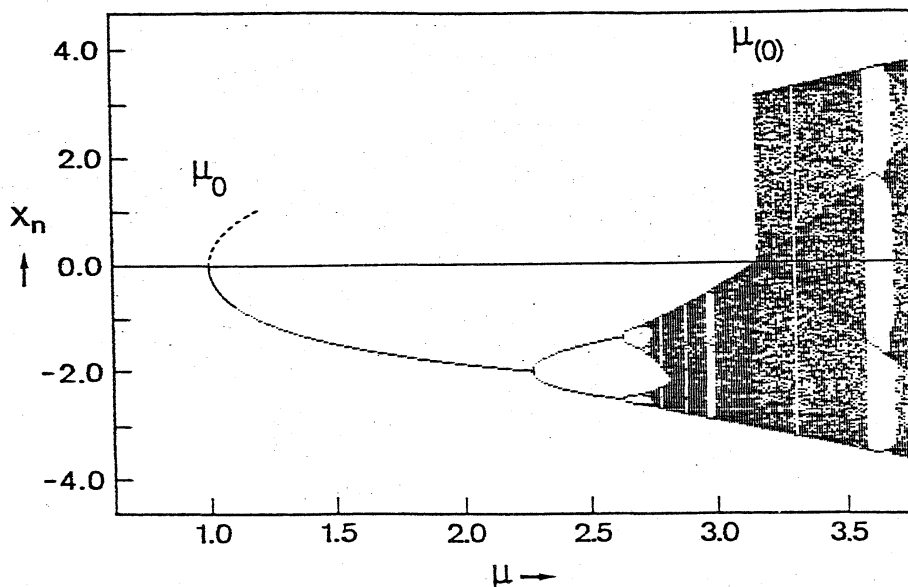
Fig. 2. Bifurcation diagram for the map, Eq. (11). At $\mu = \mu_0 = 1$, a symmetry breaking bifurcation occurs. For $\mu > \mu_0$, only the negative branch is pictured. The positive branch can be obtained by the transformation $X \to -X$. At $\mu = \mu_{(0)}$, a symmetry recovering is seen.

symmetry breaking can be seen also for the case $t_R \gamma = 0.$[11,12] We pictured in Fig. 2 only the negative branch after the bifurcation. As μ increases, each asymmetric branch undergoes period doublings followed by chaos. For $\mu < \mu_{(0)}$, the chaotic orbit is confined to the regions $X > 0$ or $X < 0$, namely, the output state is chaotic but still elliptically polarized to either direction. At $\mu = \mu_{(0)}$, the chaotic band suddenly doubles its width. There the two oppositely polarized bands collide to form a single band. Thus the symmetry broken at $\mu = \mu_0$ is recovered at $\mu = \mu_{(0)}$.

The sudden change may be viewed as 'crisis' of chaos named by Grebogi et al.[13] The crisis occurs when a strange attractor collides with a coexisting unstable fixed point or periodic orbit. In our case the situation is somewhat degenerate due to the symmetry, namely, a strange attractor collides with an unstable
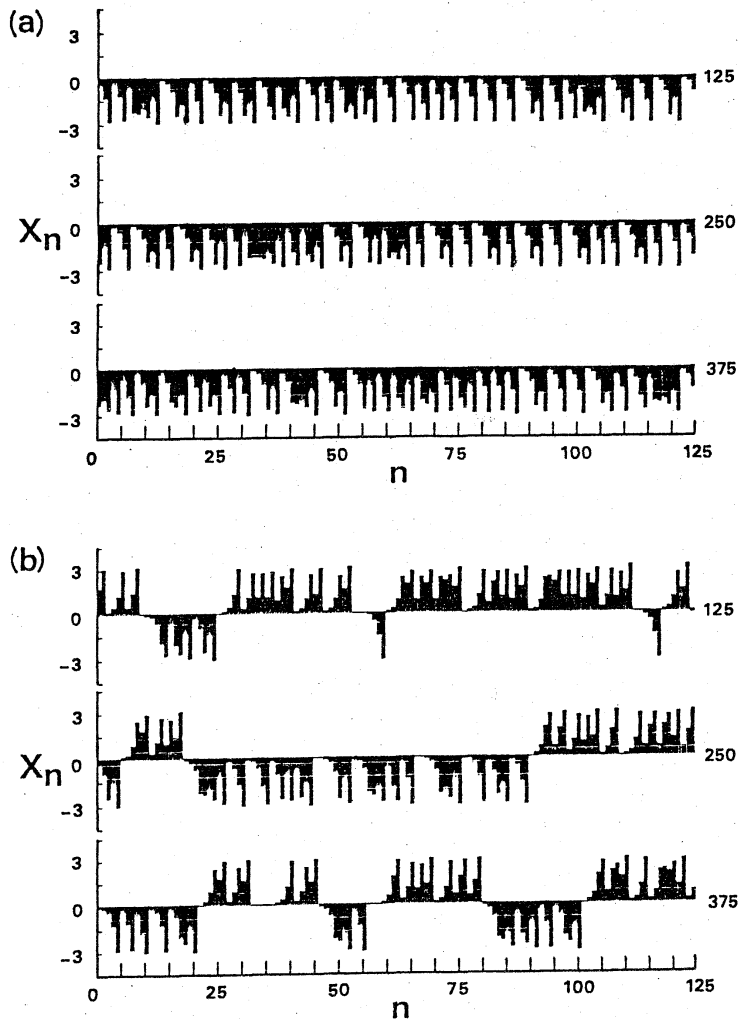
(a)

(b)

Fig. 3. Waveforms of Eq. (11) for (a) $\mu = 3.11$ (before the crisis) and (b) $\mu = 3.17$ (after the crisis). Bar graph of X_n as a function of n for 375 iteration after preiteration.

fixed point $X = 0$ and the other coexisting strange attractor simultaneously. We call the phenomenon "symmetry recovering crisis".

Figures 3(a) and (b) show examples of chaotic orbits for cases before ($\mu \lesssim \mu_{(0)}$) and after ($\mu \gtrsim \mu_{(0)}$) the crisis. The short time behaviors are the same for both cases, but in the latter crossover to the other polarized state occurs sometimes. According to Ref. 13, the average lifetime τ_{av} of each polarized state is estimated as

$$\tau_{av} \sim (\mu - \mu_{(0)})^{-1/2}. \tag{12}$$

We confirmed the estimation numerically.

IV. SIMULATION BY ANALOG CIRCUIT

In order to see how the symmetry recovering crises for Eq. (10) appear we constructed an analog circuit which simulates Eq. (10). Figure 4 shows the experimental setup. The nonlinear function sin X in Eq. (10) is approximated by $X - X^3$ and realized by two analog multipliers (Intersil ICL8013) and an operational
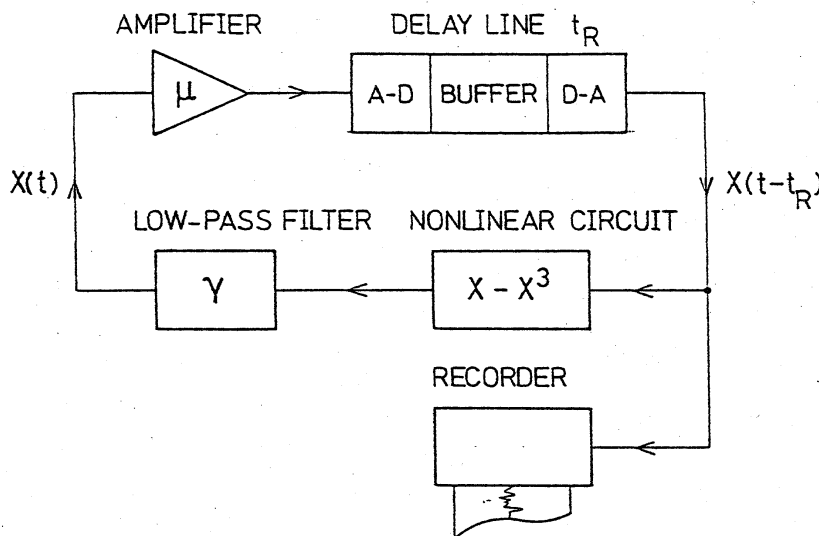

Fig. 4. Experimental setup. The analog circuit simulates the difference-differential equation (10).

amplifier. The delay t_R is given by a digital delay line equipped with a 12-bit A-D, a D-A converters, and a 4096-word buffer. The cutoff frequency γ of the low-pass filter is set at 2 Hz when we record waveforms on a strip chart recorder. We can conveniently find bifurcation points or crises on a CRT instead of the recorder

by setting $\gamma \sim 10^2 - 10^3$ Hz and shortening t_R correspondingly.

By changing t_R, we could find three distinct types of symmetry recovering crises. We named Type I, II, and II according to the order of the values t_R for which each type was observed. The critical value $\mu_{(0)}$ for crisis decreases as $t_R\gamma$ increases.

Type I: Before the crisis, rather regular pulsing is observed (Fig. 5(a)). We can see damped oscillations near X = 0 between the pulses, whose durations are different from pulse to pulse. Such oscillation is not observed when μ is far below $\mu_{(0)}$ and appears as μ approaches $\mu_{(0)}$. After the crisis (Fig. 5(b)), the crossover to the other polarized state neccessarily occurs through the damped oscillation. Thus the oscillation may be viewed as a precursor for the crisis and also as a crossover transient.

Type II: The waveform before the crisis (Fig. 6(a)) is fairly random. The bursts of periodic oscillation are precursors for the
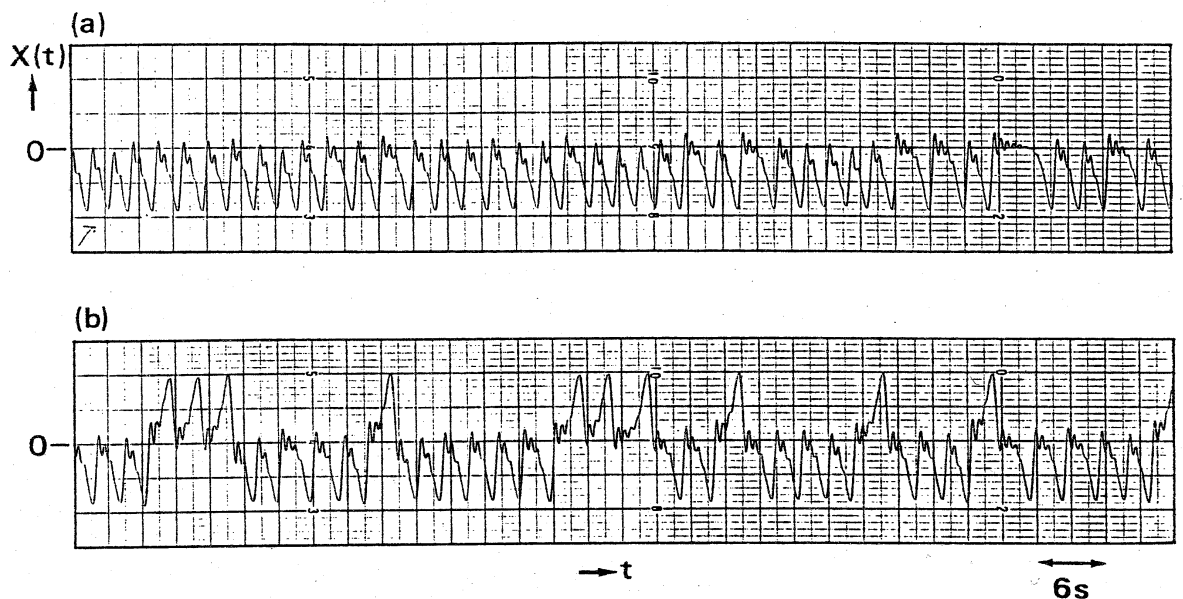

Fig. 5. Waveforms (a) before and (b) after the symmetry recovering crisis of Type I. Parameters: t_R = 0.41 s, γ = 2.0 Hz, (a) μ = 4.26; (b) μ = 4.38.
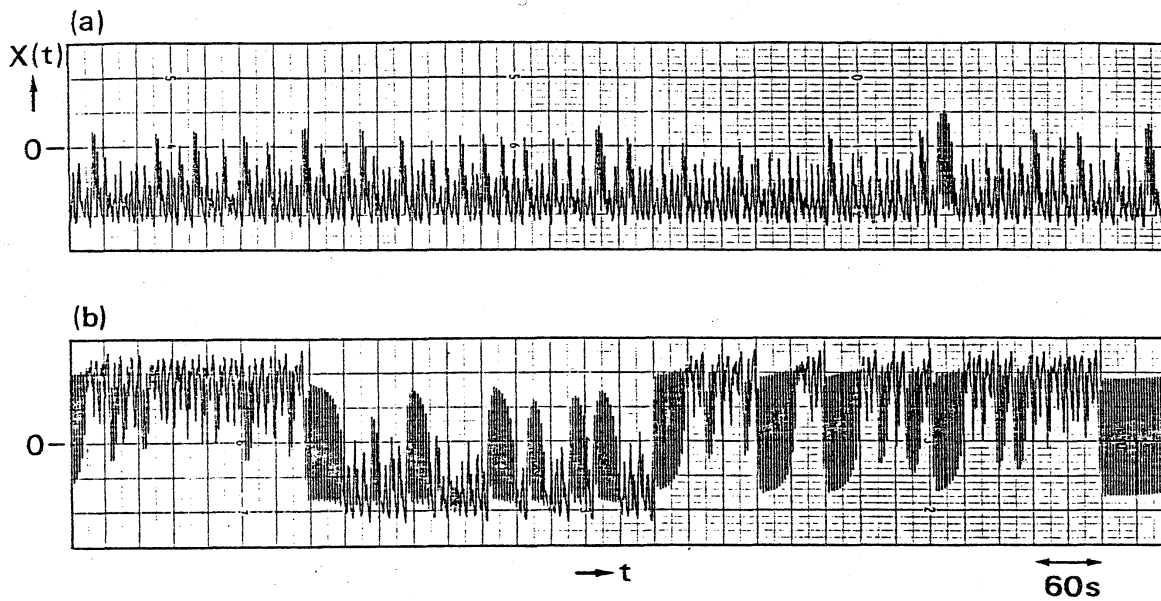
Fig. 6. Waveforms (a) before and (b) after Type II crisis. Parameters: t_R = 2.05 s, γ = 2.0 Hz, (a) μ = 2.96; (b) μ = 3.02.
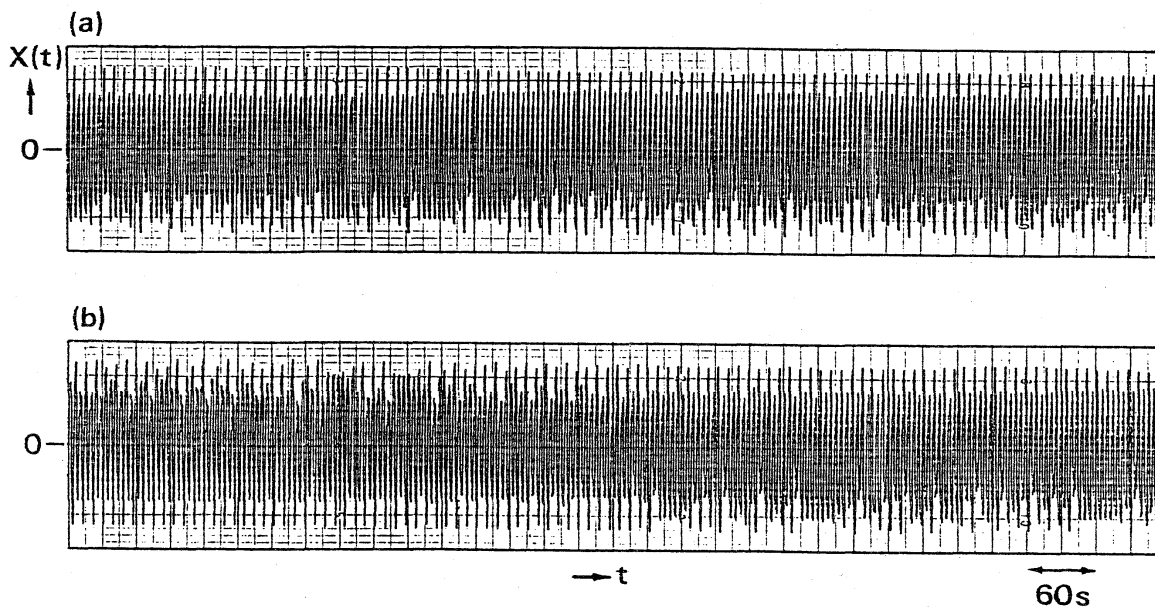

Fig. 7. Waveforms (a) before and (b) after Type III crisis. Parameters: t_R = 4.10 s, γ = 2.0 Hz, (a) μ = 2.77; (b) μ = 2.79.

crisis. They appear randomly and their duration is also random. After the crisis (Fig. 6(b)), the crossover occurs through the burst of oscillation.

Type III: At a glance there seems to be no differences between Figs. 7(a) and 7(b). However the waveform in Fig. 7(a) shows period-4 chaos which has an asymmetry with respect to X; the lower boundary is flat while the upper is not. In the middle of Fig. 7(b) we can see a crossover. No marked precursory phenomena nor crossover transients are seen for this type.

V. THE TWO DIMENSIONAL MAP MODEL

By the analog circuit simulation we have confirmed symmetry recovering crises exist for Eq. (10), as predicted by the one dimensional map model. However, the waveforms at the the three types of crises were very different from that for the one dimensional map. In this section we introduce a two dimensional difference equation and show the three types of crises occur for the equation with appropriate values of parameters.

We formally descretize Eq. (10) as

$$\gamma^{-1} \frac{X_{n+1} - X_n}{\Delta t} = -X_n + \mu F(X_{n-N}), \tag{13}$$

where N is an integer, $\Delta t = t_R/N$, $X_n = X(n\Delta t)$, and $F(X) = X(1 - X^2)$. By introducing a parameter $\alpha = \gamma\Delta t$, we obtain the following (N + 1)-dimensional difference equation:

$$X_{n+1} = (1 - \alpha)X_n + \alpha\mu F(X_{n-N}), \tag{14}$$

In the limit $\alpha \to 0$, N and t_R = constant, Eq. (14) approximates the differential equation (10) with $t_R = 0$. For the case $\alpha = 1$, Eq. (14) reduces to the one dimensional difference equation (11). So α

is a parameter which connects a difference equation and a differential equation as $t_R\gamma$ does in Eq. (10).

Here we crudely set $N = 1$ in Eq. (14) and obtain a two dimensional difference equation:[15]

$$X_{n+1} = (1 - \alpha)X_n + \alpha\mu F(Y_n),\qquad(15a)$$

$$Y_{n+1} = X_n,\qquad(15b)$$

where $Y_n = X_{n-1}$. The equation is invariant under the transformation $(X, Y) \to (-X, -Y)$.

Surprisingly we could find the three types of crises in this oversimplified equation. In Figs. 8, 9, and 10, we show the waveforms near the crises. The clear correspondences to Figs. 5, 6, and 7 are seen. Especially the same precursors and crossover transients appear for Types I and II. Type I was found for smaller values of α (near differential-equation limit), Type III was for $\alpha \lesssim 1$ (near difference equation limit), and Type II was in the middle. The order is consistent with the results in the previous section.

As described in Sec. III, for the one dimensional map, the symmetry crisis is undergone when a strange attractor collides with an unstable fixed point and the other strange attractor. Here we investigate the situation for the two dimensional cases. Figure 11, 12, and 13 show the strange attractors near the crises of Type I, II, and III respectively.

Type I: Figure 11(a) shows the strange attractor just before the crisis. The other coexisting attractor is obtained by the transformation $(X, Y) \to (-X, -Y)$. The two limit-cycle like
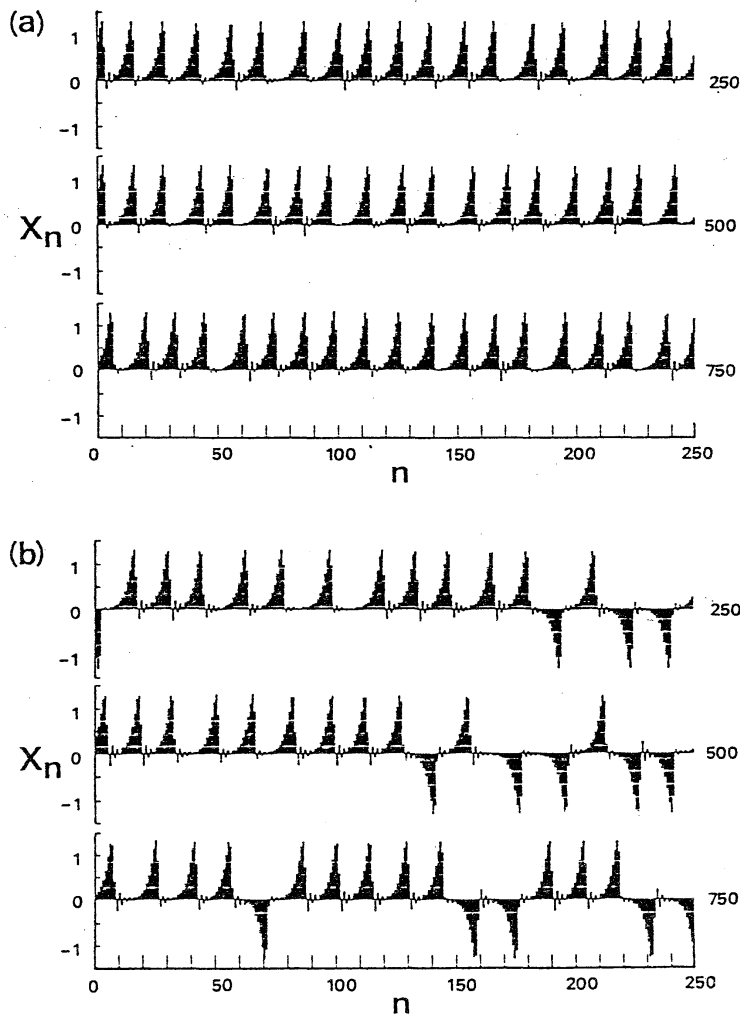
Fig. 8. Calculated waveforms (a) before and (b) after Type I crisis. Graph of X_n of Eq. (15) for 750 iteration after preiteration. Parameters: $\alpha = 0.1$, (a) $\mu = 10.24$; (b) $\mu = 10.30$.

attractors are about to touch each other near the origin. A round trip of the cycle forms a pulse in Fig. 8. At $\mu = \mu_{(0)}$, two attractors are merged and for $\mu \stackrel{<}{\sim} \mu_{(0)}$, an orbit on an attractor can go over to the other.

Figure 11(b) is an enlargement of part of Fig. 11(a). The two attractors are clearly separated. The regular structure of the attractors is a reflection of the existence of a fixed point (0,0) of Eq. (15). By the stability analysis, we can see that the eigenvalues ρ_1, ρ_2 of the linearized map at (0,0) satisfy the relations: $-1 < \rho_1 = -0.66 < 0$, $1 < \rho_2 = 1.56$. The corresponding
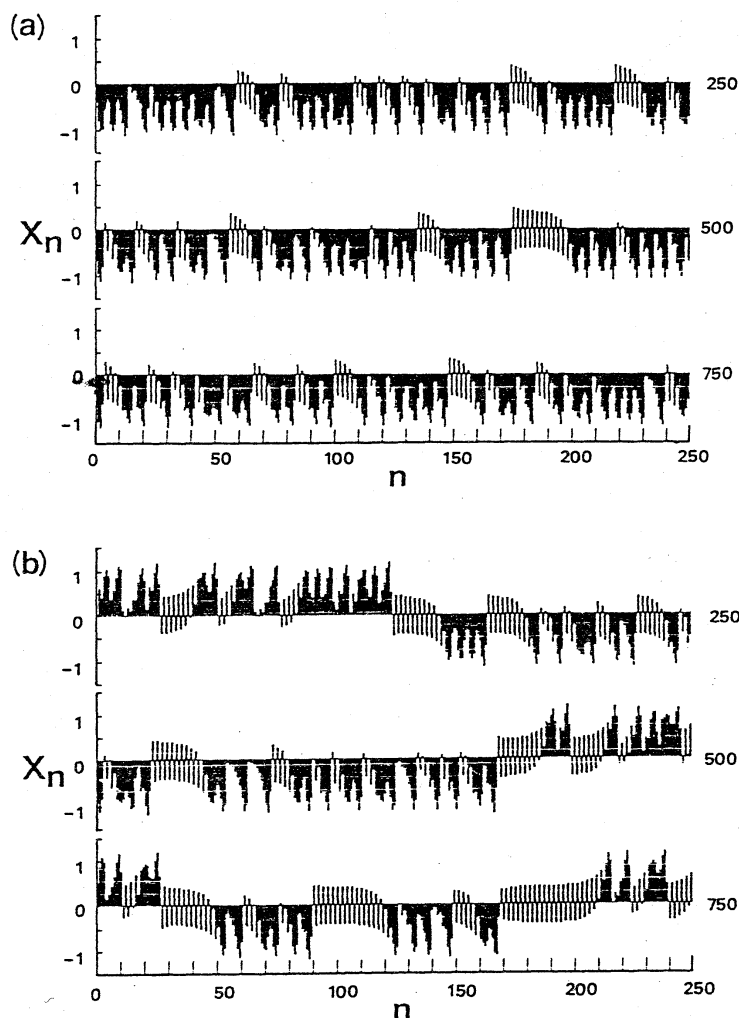
(a)

Fig. 9. Calculated waveforms (a) before and (b) after Type II crisis. Parameters: $\alpha = 0.5$, (a) $\mu = 3.54$; (b) $\mu = 3.57$.

eigenvectors are $\vec{u}_1 = -0.66\hat{x} + \hat{y}$, $\vec{u}_2 = 1.56\hat{x} + \hat{y}$. According to the classification of the fixed points in Ref. 15, the point (0,0) is DR^1 for this parameter values. To simplify the situation, we consider a composite map $T^{(2)} = T \circ T$ where T is a map defined by Eq. (15). The point is a saddle (D^2) for $T^{(2)}$ since $0 < \rho_1^2 < 1 < \rho_2^2$. We use schematic illustrations in Fig. 14 to give general discussions. The point S is a saddle, and C_s and C_u are the stable and unstable invariant curves respectively. The eigenvectors $\vec{u}_1$ and $\vec{u}_2$ are tangent to C_s and C_u at S. When $\mu < \mu_{(0)}$ (Fig. 14(a)), C_s is also the boundary separating the basins of attraction for the
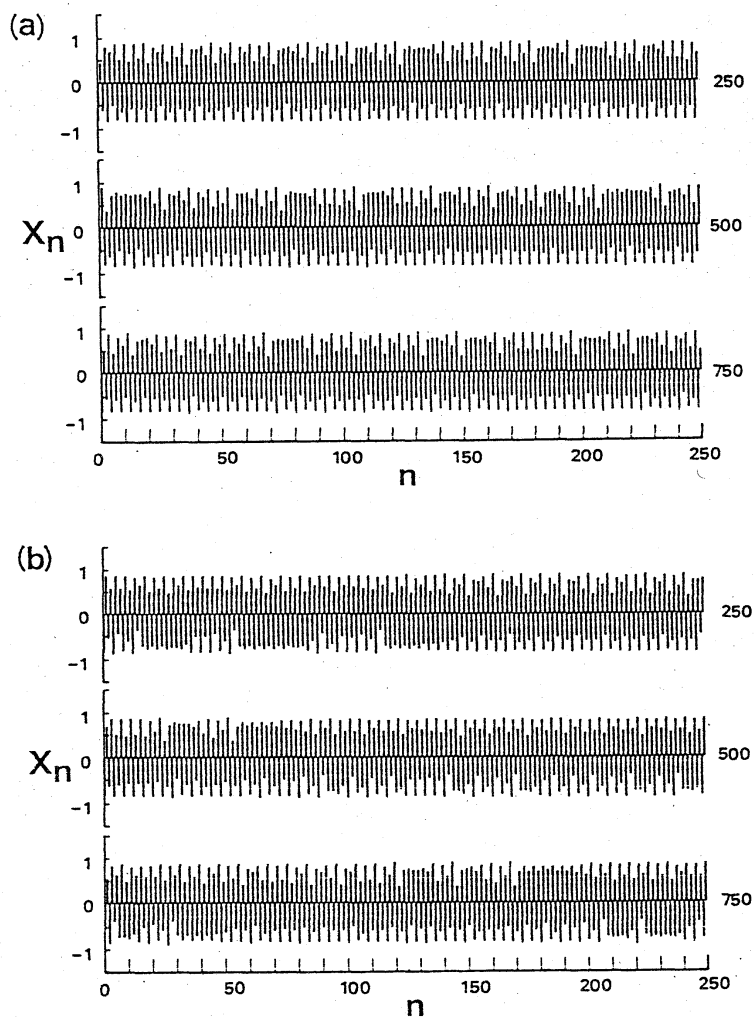
(a)

(b)

Fig. 10. Calculated waveforms (a) before and (b) after Type III crisis. Parameters: $\alpha = 0.85$, (a) $\mu = 2.944$; (b) $\mu = 2.946$.

two attractors. The region R_1, which is mapped from somewhere in the attractor, is mapped to R_2, to R_3, ... , successively, and at last repelled back along C_u. When the crisis is reached, R_1 touches the boundary C_s, as a result, R_i ($i = 2,3,...$) touch C_s and R_∞ touches to S. As seen in Fig. 14(b), for $\mu \gtrsim \mu_{(0)}$, points in R_1 over C_s are repelled over to the other attractors along C_u after some iterations of the map.

Near the crisis, a point mapped close to C_s in R_1 will need many iterations to be repelled away from S, namely, the orbit is trapped to S temporarily. If S is a period-n point (a fixed point

b.

a.
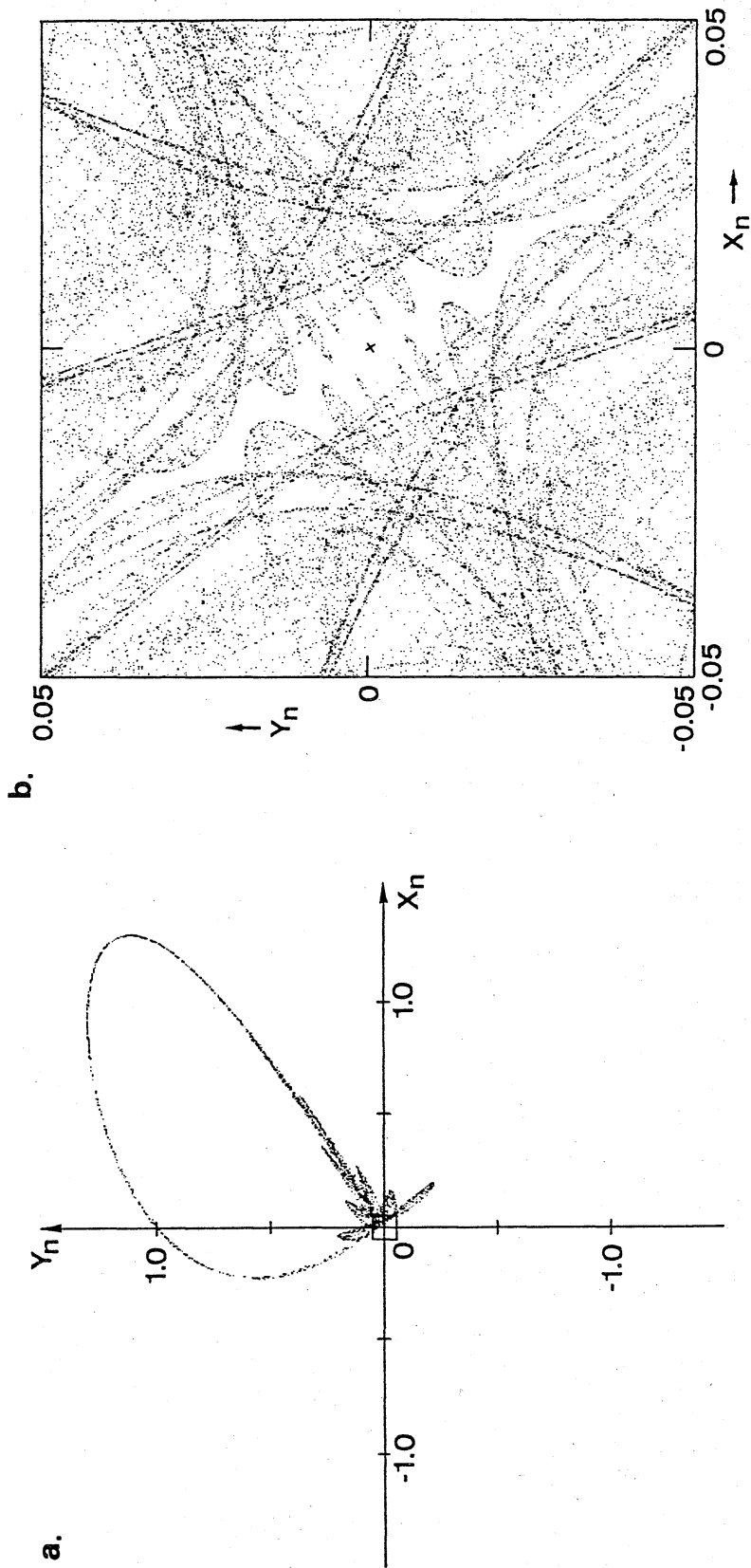
Fig. 11. (a) Chaotic attractor for Eq. (15) before Type I crisis. An initial point is chosen and its orbit is plotted after preiteration. The other coexisting attractor is obtained by the transformation $(X, Y) \rightarrow (-X, -Y)$. Parameters: $\alpha = 0.1$, $\mu = 10.24$.

(b) Blowup of the boxed region in (a). Both coexisting attractors are plotted. A cross represents an unstable fixed point at $(0,0)$. Parameters: $\alpha = 0.1$, $\mu = 10.244$.
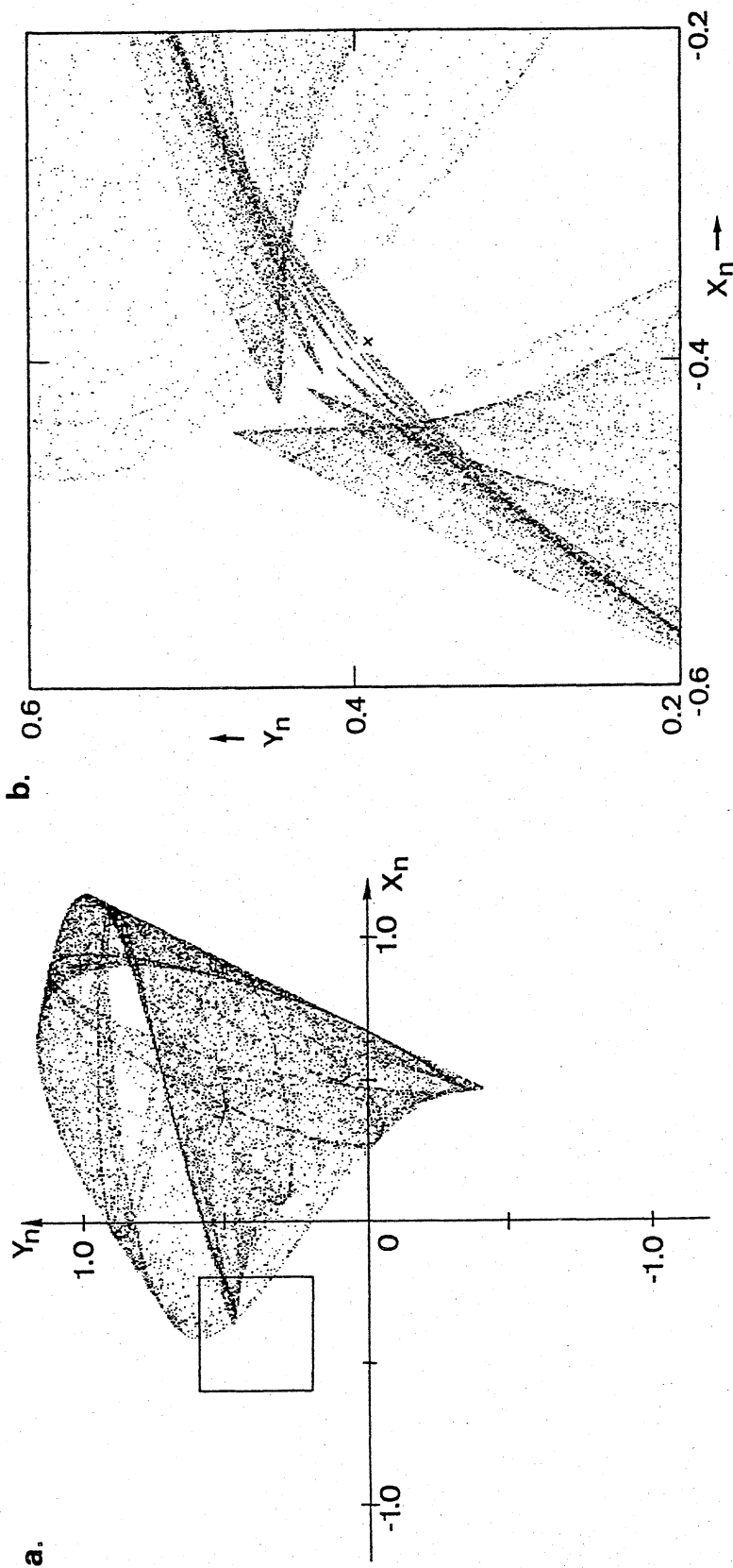
Fig. 12. (a) Chaotic attractor for Eq. (15) before Type II crisis. The other coexisting attractor is obtained by the transformation (X, Y) → (-X, -Y). Parameters: α = 0.5, μ = 3.51.
(b) Blowup of the boxed region in (a). Both coexisting attractors are plotted. Parameter μ is closer to $μ_{(0)}$ than in (a). A cross represents one of unstable period-2 points at (±0.39, ∓0.39). Parameters: α = 0.5, μ = 3.541.
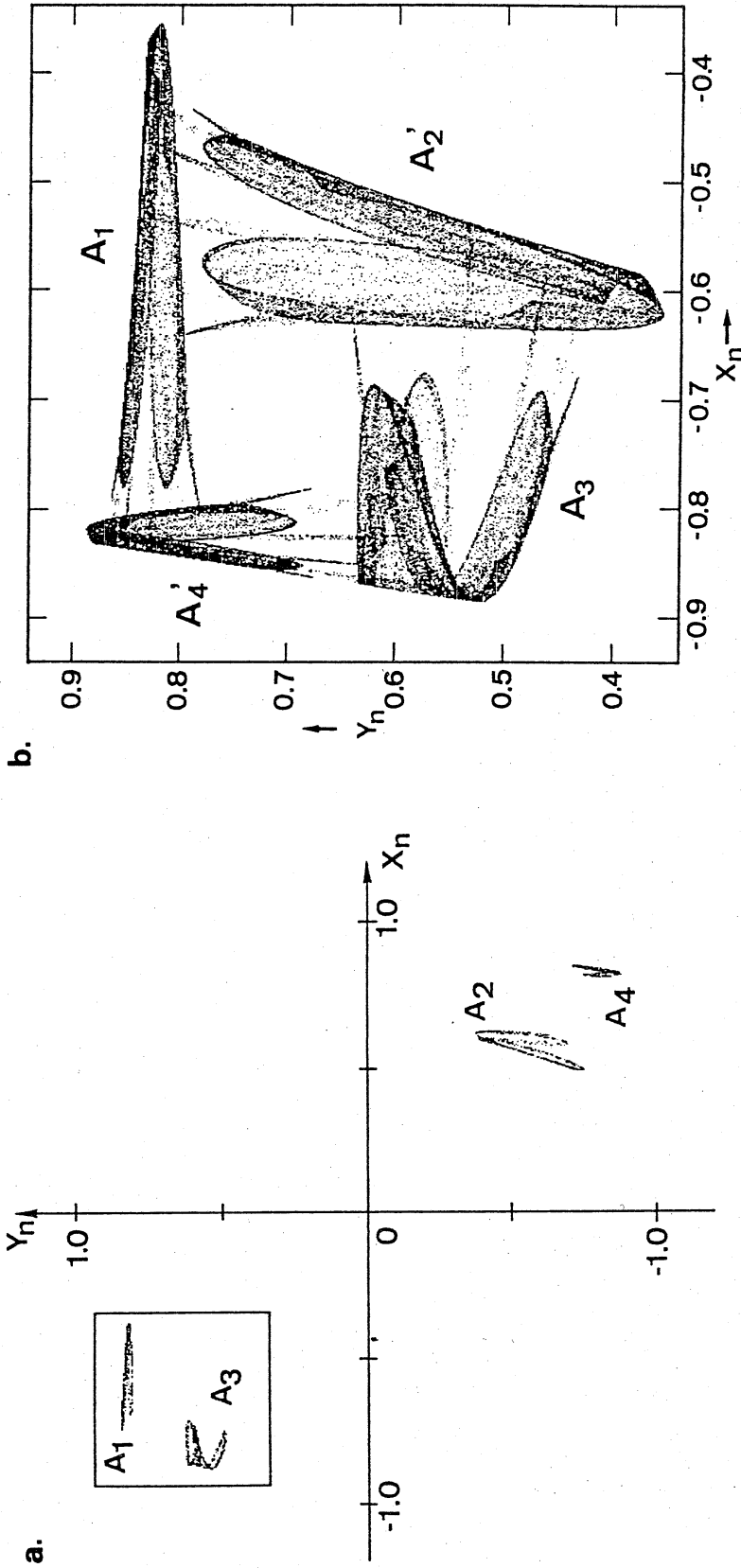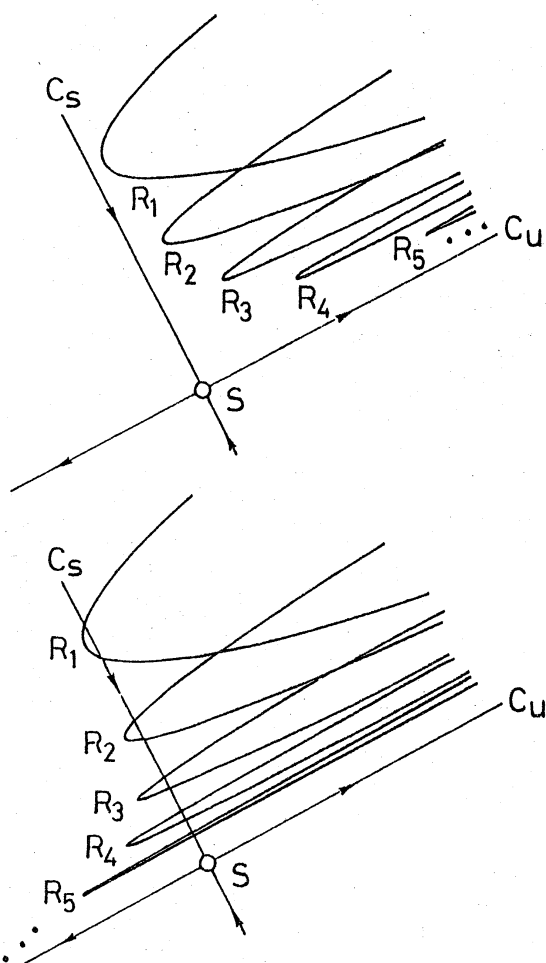
Fig. 13. (a) Four-piece chaotic attractor (A_1, A_2, A_3, A_4) for Eq. (15) before Type III crisis. The other coexisting attractor (A_1', A_2', A_3', A_4') is obtained by the transformation (X, Y) → (-X, -Y). Parameters: α = 0.85, μ = 2.93.

(b) Blowup of the boxed region in (a). Parameter μ is above the critical value for the crisis, therefore attractor pieces are merged to form a two-piece attractor. Parameters: α = 0.5, μ = 2.946.

Fig. 14. Schematic illustration for crisis of chaotic attractor through a saddle point S. (a) Before and (b) after the crisis, the regions R_i are mapped to R_{i+1}. C_s and C_u represent the stable and unstable invariant curves of S respectively.

for $T^{(n)}$), one will observe n-periodic oscillation with some duration. Such phenomena will be seen as precursor of crisis when $\mu \overset{<}{\sim} \mu_{(0)}$ and as crossover transient when $\mu \overset{>}{\sim} \mu_{(0)}$.

Type II: A wide-spread attractor is seen in Fig. 12(a). The other coexisting attractor lies symmetrically. The touch occurs near period-2 points (± 0.39, ∓ 0.39), whose stability is D^2. Figure 12(b) show a blowup, where we see the same structure as in Fig. 14(a). We can hardly see the regular structure in Fig. 12(a) because μ is not so close to $\mu_{(0)}$. The bursts of oscillation seen in Fig. 9 mean that the orbit is trapped to the period-2 points.

The closer the point is dropped to the stable invariant curve, the longer the regular oscillation continues.

Type III: The situation is rather complicated than in Types I and II. Before the crisis, two four-piece strange attractors are coexisting. In Fig. 13(a), only the attractor (A_1, A_2, A_3, A_4) is pictured. The other attractor $(A_1{}', A_2{}', A_3{}', A_4{}')$ is obtained by the transformation $(X, Y) \rightarrow (-X, -Y)$. An orbit cycles as $A_1 \rightarrow A_2 \rightarrow A_3 \rightarrow A_4 \rightarrow A_1$ or as $A_1{}' \rightarrow A_2{}' \rightarrow A_3{}' \rightarrow A_4{}' \rightarrow A_1{}'$, and gives period-4 chaos as in Fig. 10(a). The flat boundary in the waveform comes from the fact that the attractor pieces A_4 and $A_4{}'$ have narrower width in the X-direction than the other pieces.

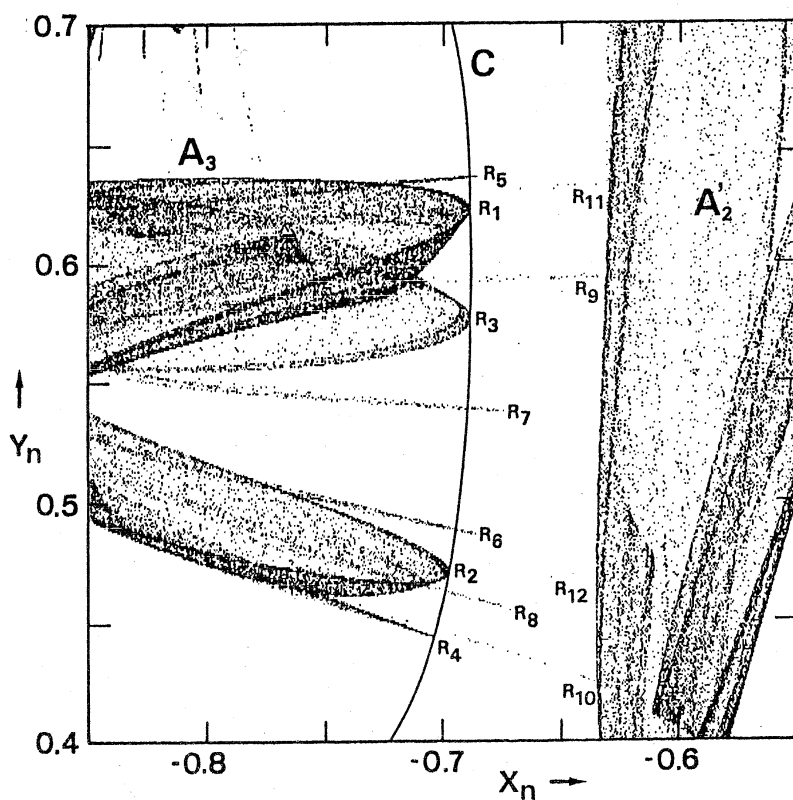After the crisis occurs, the two attractors are merged as seen

Fig. 15. Blowup of part between A_3 and $A_2{}'$ of Fig. 14(b). Parameter μ is above $\mu_{(0)}$. The regions R_i are mapped to R_{i+1} by $T^{(4)}$. C represents an unstable invariant curve. Parameters: $\alpha = 0.85$, $\mu = 2.2447$.

in Fig. 13(b). To see how the merging occurs a further blowup is

given in Fig. 15. Between A_3 and A_2', there exists an invariant curve C, which forms a part of the basin boundary before the crisis. We can see that the regions R_i (i = 1, 2, ...) are mapped to R_{i+1} by $T^{(4)}$. In the course of iterations of the map, the regions are stetched in the direction across the curve C, and their tips are attracted to A_2'. The regions R_i (i > 12) can't be seen for the points are so dispersed by the stretching.

The configuration of R_i along C can be understood as follows. Restriction $T^{(4)}$ to the invariant curve C gives a one dimensional unimodal map which exhibits period-2 chaos. So the configuration of R_i is somewhat erratic, although we can group them into (R_{2n-1}) and (R_{2n}) (n = 1, 2, ...).

It is seen, from the theory of unimodal map, that there exist infinite numbers of unstable fixed points on C; one UR^4, two UR^8, four UR^{16}, ... Therefore we may say the crisis occurs through UR^k (k = 2n, n = 0, 1, 2, ...). Here, however, we are tempted to modify the Grebogi's definition of crises as 'a collision of a chaotic attractor to an unstable invariant curve'.

VI. CONCLUSION

In summary we have investigated the symmetry recovering crises of chaos in a polarization-related optically bistable system. Through the crises, chaotic states having the polarization asymmetry, which is inherited from the first bifurcation, jumps back to a symmetric state. We have found three distinct types of the crises by changing the parameter $t_R\gamma$. All of the waveforms near these crises are very different from that for the one dimensional map model which has been used to analyze difference-

differential equations such as Eq. (10). Whereas a two dimensional map model we introduced gives good qualitative explanations to the three types of crises.

As Grebogi et al.[13] said, crises occurs when a chaotic attractor collides with an unstable fixed point or an unstable periodic orbit. In our cases of Types I, II, and III, collisions to the unstable fixed points of types DR^1, D^2, and UR^{4k} ($k = 2^n$) occur. For Types I and II unstable fixed point has a stable invariant curve in addition to an unstable invariant curve. The stable curve forms a part of the basin boundary which separate the paired chaotic attractors before the crisis. Along the stable invariant curve, regular structures are formed just before and after the crisis. For Type III, a one dimensional map on the invariant curve, which yields chaos, gives marked structure to the strange attractors near the crisis.

Perhaps there exist other types of symmetry recovering crises than those we treated here. (For example Fig. 3(c) in Ref. 16 suggests another type which is close to Type III.) Some of them may need models in higher dimensions. Even for such cases, types of the unstable fixed point will characterize the crises. Statistical behavior near each crisis such as Eq. (12) should be investigated.

Finally we estimate experimental parameters to observe the phenomena in an all optical system. The Na system of Ref. 12 with which we have observed the symmetry breaking bifurcation should be modified. The delay t_R can be provided by an optical fiber with sufficient length L. We see from Eq. (10) and the requirement $t_R \gamma \gtrsim 1$ that the required power density I_0 is inversely proportional to t_R, or L. For L = 1 km (t_R = 6 µs), I_0 is

estimated to be 1 ~ 10 W/mm^2, which is not unrealistic value

considering the use of a multi-mode laser.

REFERENCES

1. K. Ikeda, Opt. Commun. 30, 257 (1979); K. Ikeda, H. Daido, and O. Akimoto, Phys. Rev. Lett 45, 709 (1980).

2. K. Ikeda and O. Akimoto, Phys. Rev. Lett 48, 617 (1982); K. Ikeda, K. Kondo, and O. Akimoto, Phys. Rev. Lett 49, 1467 (1982).

3. H. M. Gibbs, F. A. Hopf, D. L. Kaplan, and R. L. Shoemaker, Phys. Rev. Lett 46, 474 (1981); F. A. Hopf, D. L. Kaplan, H. M. Gibbs, and R. L. Shoemaker, Phys. Rev. A 25, 2172 (1982); M. W. Derstein, H. M. Gibbs, F. A. Hopf, and D. L. Kaplan, Phys. Rev. A 26, 3720 (1982); M. W. Derstein, H. M. Gibbs, F. A. Hopf, and D. L. Kaplan, Phys. Rev. A 27, 3200 (1983).

4. H. J. Carmichael, C. M. Savage, and D. F. Walls, Phys. Rev. Lett 50, 163 (1983); H. J. Carmichael, in Laser Physics, Lecture Notes in Physics 182, eds. J. D. Harvey and D. F. Walls (Springer, Berlin 1983) p. 64.

5. H. Nakatsuka, S. Asaka, H. Itoh, K. Ikeda, and M. Matsuoka, Phys. Rev. Lett 50, 109 (1983).

6. T. Poston, D. F. Walls, and P. Zoller, Optica Acta 29, 1691 (1982).

7. J. V. Moloney and H. M. Gibbs, Phys. Rev. Lett 48, 1607 (1982); D. W. Mc Laughlin, J. V. Moloney, and A. C. Newell, Phys. Rev. Lett 51, 75 (1983).

8. M. Kitano, T. Yabuzaki, and T. Ogawa, Phys. Rev. Lett 46,

926 (1981); and Phys. Rev. A 24, 3156 (1981).

9. C. M. Savage, H. J. Carmichael, and D. F. Walls, Opt. Commun. 42, 211 (1982); F. T. Arecchi, J. Kurman, and A. Politi, Opt. Commun. 44, 421 (1983);

10. S. Cecchi, G. Giusfredi, E. Petriella, and P. Salieri, Phys. Rev. Lett 49, 1928 (1982); F. Mitschke, J. Mlynek, and W. Lange, Phys. Rev. Lett 50, 1660 (1983); W. J. Sandle and M. W. Hamilton, in Laser Physics, Lecture Notes in Physics 182, eds. J. D. Harvey and D. F. Walls (Springer, Berlin 1983) p. 54.

11. T. Yabuzaki, M. Kitano, and T. Ogawa, Proceedings of Lasers '82, ed. R. Powell (Springer, Berlin 1983).

12. T. Yabuzaki, T. Okamoto, M. Kitano, and T. Ogawa (to be published).

13. C. Grebogi, E. Otto, and J. A. York, Physica 7D, 181 (1983); and Phys. Rev. Lett 48, 1507 (1982).

14. M. Kitano, T. Yabuzaki, and T. Ogawa, Phys. Rev. Lett 50, 713 (1983);

15. 川上　博：京都大学数理解析研究所講究録 No.370, 88 (1979).

16. F. T. Arecchi and F. Lisi, Phys. Rev. Lett 49, 94 (1982).